Angular dependence of hot-electron transport through a two-dimensional electron-gas layer

R.-J. E. Jansen and Behnam Farid
Cavendish Laboratory, Department of Physics, University of Cambridge, Madingley Road, Cambridge CB3 0HE, United Kingdom

M. J. Kelly
Department of Physics, University of Surrey, Guildford, Surrey GU2 5XH, United Kingdom
(Received 28 December 1992)

We present an analysis of the angular dependence of hot-electron transport through a zero-temperature two-dimensional electron gas (2DEG), as can be realized experimentally in semiconductor structures under applied magnetic fields. We calculate the scattering probability and energy loss as functions of energy and angle of incidence of the hot electrons impinging on a 2DEG of density $n_s = 10^{16}$ m^{-2}. For high injection energies the total scattering probability and the energy loss show an inverse cosine behavior, while for lower injection energies the scattering exhibits a sudden decrease due to the disappearance of the 2DEG-plasmon scattering channel. We discuss the implications of our findings for the operation of 2DEG-base hot-electron transistors.

I. INTRODUCTION

The advent of the two-dimensional electron-gas-base hot-electron transistor (2DEGBHET) has made accessible the scattering processes of hot electrons impinging on a 2DEG. The transistor geometry (see Fig. 1) allows a wide range of experiments to be performed: the energy, angle of incidence, and density of the injected electrons can be varied separately from any variation in the temperature, density, and drift velocity of the 2DEG.[1–4] In an initial theoretical investigation,[5] we obtained close agreement with the experimental value of the transfer ratio (i.e., that fraction of hot injected electrons that are collected after passing through the 2DEG base region) in the absence of magnetic fields. Electrons emitted into the base at low temperatures have a typical energy of 100–300 meV and velocities in a narrow forward cone with axis perpendicular to the plane of the 2DEG. Under an applied magnetic field in the plane of the 2DEG in the base region, the Lorentz force induces a curved trajectory for the injected electrons as they transit the base, thus changing the angle of incidence of the hot electrons with the 2DEG. We extend our earlier work[5] to analyze the angular dependence of the hot-electron 2DEG interactions. Whereas all previous hot-electron spectroscopy involved a homogeneous three-dimensional electron-gas base, the angle of incidence of the hot electron with the base electron gas has added significance when dealing with the spectroscopy of the intrinsic inhomogeneous base of the 2DEGBHET.

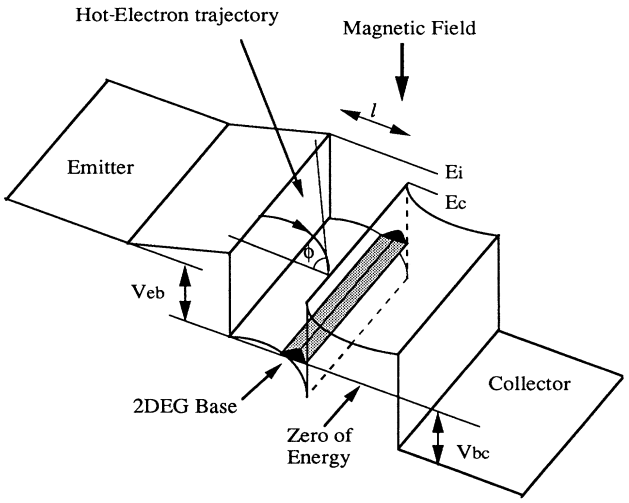

FIG. 1. A schematic diagram of the 2DEGBHET showing (i) the important voltages that describe its operation, (ii) the effect of the Lorentz force on the trajectory of an injected electron, and the angle of incidence of the hot electron with the 2DEG, and (iii) the incidence and collection energies E_i and E_c, respectively. The zero of energy is taken to coincide with the Fermi energy of the 2DEG in the base.

In this paper we present the theory and the results of our numerical studies for hot-electron transport through a 2DEG in a 2DEGBHET. The former is given in Sec. II and the latter are presented and discussed in Sec. III. Conclusions and a summary of this work are given in Sec. IV. Some of the details of our calculations can be found in an Appendix that follows the last section.

II. THEORY

The electron transport properties through a 2DEG are described in terms of the scattering-probability distribution $\theta(p_\alpha, p_{\alpha'}, \mathbf{P}, \mathbf{P}')$ of an incoming electron being scattered by the 2DEG from an initial state $|p_\alpha, \mathbf{P}\rangle$ to a final state $|p_{\alpha'}, \mathbf{P}'\rangle$. We consider the 2DEG to be in the x,y plane (i.e., $z=0$) and the impinging electron to have initial momentum p_α in the z and $\mathbf{P}=(P_x, P_y)$ in the x,y directions (see Fig. 2). We denote the momenta of the electron after the scattering event by a prime. In a hot-electron transistor the fraction of electrons being captured in the base depends on the emitter-base barrier, i.e.,

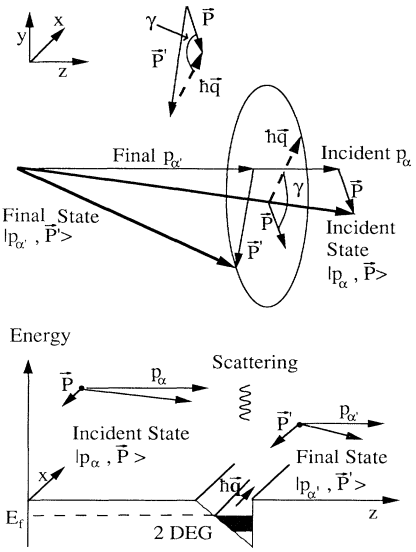

FIG. 2. Schematic representation of a hot electron impinging on a 2DEG layer and scattering from initial state $|p_\alpha,\mathbf{P}\rangle$ to final state $|p_{\alpha'},\mathbf{P}'\rangle$. p_α and $\mathbf{P}$ describe the momentum of the hot electron, respectively, in the z direction and in the x-y plane. $\hbar\mathbf{q}=\mathbf{P}-\mathbf{P}'$ is the momentum exchanged with the 2DEG and γ the angle between $\mathbf{P}$ and $\hbar\mathbf{q}$. Note that due to rotational symmetry along the z direction, the excitations of the 2DEG of momentum $\hbar\mathbf{q}$ all lie on the circle indicated. The corresponding excitation energies depend on the angle γ [see Eq. (6)]. The top figure shows how the initial and final momenta of the hot electron and of the 2DEG excitation are related to each other. The bottom figure shows schematically the hot-electron scattering with the 2DEG.

injection energy E_i, the base-collector barrier, i.e., collection energy E_c, and angle of incidence ϕ (see Fig. 1). We investigate this capture theoretically using the scattering-probability distribution θ to obtain the fraction of electrons scattered into the base, i.e., the base scattering probability $P(E_c,E_i,\phi)$, and the energy loss $E_{\rm loss}(E_i,\phi)$, with varying injection and collection energies, and incidence angles. The forward-scattering probability $P^>(E_c,E_i,\phi)$ for an injection energy E_i and collection energy E_c is found by summing the scattering-probability distribution over all the energetically allowed forward-scattering states $|p_{\alpha'},\mathbf{P}'\rangle$, with $p_{\alpha'}>0$, for which the energy in the z direction $E_z(p_{\alpha'})$ is less than the collection energy E_c,

$$P^>(E_c,E_i,\phi)=\sum_{\substack{p_{\alpha'}>0\\ E_z(p_{\alpha'})<E_c}}\sum_{\mathbf{P}'}\theta(p_\alpha,p_{\alpha'},\mathbf{P},\mathbf{P}')\ . \tag{1}$$

Note that the injection energy is equal to the incident hot-electron energy, $E_i=E(p_\alpha,\mathbf{P})$, and that the incidence angle is given by $\phi=\arctan\{|\mathbf{P}|/p_\alpha\}$. The backward-scattering probability $P^<(E_c,E_i,\phi)$ is found similarly by summing over all the backscattering states, with $p_{\alpha'}<0$. The sum of both the forward- and backward-scattering probabilities is the base scattering probability, i.e., $P(E_c,E_i,\phi)=P^>(E_c,E_i,\phi)+P^<(E_c,E_i,\phi)$.

The energy loss for an incident state $|p_\alpha,\mathbf{P}\rangle$ is the weighted sum of the scattering probability over all the different scattering channels with the appropriate energy loss,

$$E_{\rm loss}(E_i,\phi)=\sum_{p_{\alpha'}}\sum_{\mathbf{P}'}\theta(p_\alpha,p_{\alpha'},\mathbf{P},\mathbf{P}')[E(p_\alpha,\mathbf{P})-E(p_{\alpha'},\mathbf{P}')]\ . \tag{2}$$

In calculating the energy loss of the impinging hot electrons, both "down-" and "up-scattering" processes have to be taken into account. In the former case the energy in the z direction $E_z(p_\alpha)$ is lost to the 2DEG by increasing the momentum in the x,y direction ($|\mathbf{P}'|>|\mathbf{P}|$). The latter scattering processes cause energy increase in the z direction through a transition to a lower lateral momentum state, i.e., $|\mathbf{P}'|<|\mathbf{P}|$. Both these scattering events will contribute to an overall loss of the total hot-electron energy $E(p_\alpha,\mathbf{P})$ and have to be taken into account when calculating the energy loss $E_{\rm loss}(E_i,\phi)$, while only the down-scattering processes have to be considered for the calculation of the base scattering probability $P(E_c,E_i,\phi)$.

The scattering-probability distribution $\theta(p_\alpha,p_{\alpha'},\mathbf{P},\mathbf{P}')$ for a scattering event from state $|p_\alpha,\mathbf{P}\rangle$ to state $|p_{\alpha'},\mathbf{P}'\rangle$ is obtained by dividing the scattering rate W [see next paragraph and Eq. (4)] for this process by the incident rate of electrons, which for this geometry is equal to p_α/m^*L_z, to give

$$\theta(p_\alpha,p_{\alpha'},\mathbf{P},\mathbf{P}')=\frac{m^*L_z}{p_\alpha}W(p_\alpha,p_{\alpha'},\mathbf{P},\mathbf{P}')\ , \tag{3}$$

in which m^* is the effective mass of an incoming hot electron and L_z denotes the normalization length in the z direction of the system in which we perform our calculations. For practical purposes we consider the 2DEG to be enclosed in a cuboid of linear dimensions L_x, L_y, and L_z, and take for the wave function of an impinging hot electron, assumed to be little perturbed by the 2DEG-confining barriers, a normalized plane wave of the form $\exp[i\{P_x x+P_y y+p_\alpha z\}/\hbar]/\sqrt{LxLyLz}$. Our approach allows for other, more accurate, hot-electron wave functions to be used if necessary.

We adopt here the same formalism that we developed and applied previously in studying normally incident hot electrons.[5] From first-order time-dependent perturbation theory, as embodied in the Fermi golden rule, and the imaginary part of the inverse of the dielectric function, which is characterized by the configuration of the electronic states in the 2DEG, the Coulomb scattering rate $W(p_\alpha,p_{\alpha'},\mathbf{P},\mathbf{P}')$ for a hot electron scattering from the initial state $|p_\alpha,\mathbf{P}\rangle$ to the final state $|p_{\alpha'},\mathbf{P}'\rangle$ is found to be

$$W(p_\alpha,p_{\alpha'},\mathbf{P},\mathbf{P}')=\frac{-1}{\hbar}\int d^3r\,d^3r'd^3r''\langle p_\alpha,\mathbf{P}|\hat{\rho}_h(\mathbf{r})|p_{\alpha'},\mathbf{P}'\rangle \times{\rm Im}[\epsilon^{-1}(\mathbf{r},\mathbf{r}';E(p_\alpha,\mathbf{P})-E(p_{\alpha'},\mathbf{P}'))]V(\mathbf{r}'-\mathbf{r}'')\langle p_{\alpha'},\mathbf{P}'|\hat{\rho}_h(\mathbf{r}'')|p_\alpha,\mathbf{P}\rangle\ , \tag{4}$$

in which ϵ^{-1} stands for the inverse dielectric function and $\hat{\rho}_h(\mathbf{r})$ denotes the hot-electron number density operator [cf. Eqs. (1)–(4) of Ref. 5 for details]. Within this formalism exchange and correlation effects between the hot electron and the 2DEG are omitted, i.e., hot electrons are treated as distinguishable from the electrons in the 2DEG. Using the translational invariance in the x,y direction, the expression for the hot-electron scattering rate $W(p_\alpha,p_{\alpha'},\mathbf{P},\mathbf{P}')$ can be simplified by Fourier transforming it in these directions. The resulting expression is evaluated by making a number of approximations: (i) as mentioned above, we use plane waves to describe the hot electrons such that the hot-electron density-operator matrix element $\langle p_\alpha,\mathbf{P}|\hat{\rho}_h(\mathbf{r})|p_{\alpha'},\mathbf{P}'\rangle$ in Eq. (4) becomes

$$\langle p_\alpha,\mathbf{P}|\hat{\rho}_h(\mathbf{r})|p_{\alpha'},\mathbf{P}'\rangle = \frac{\exp[i\{(P_x'-P_x)x+(P_y'-P_y)y+(p_{\alpha'}-p_\alpha)z\}/\hbar]}{L_xL_yL_z}, \tag{5}$$

(ii) we neglect phonons and thus their contribution to the dielectric function, (iii) we limit ourselves to a one-subband zero-temperature 2DEG, with sheet density n_s, (iv) we neglect higher subbands in calculating the polarization function for the dielectric function, and (v) we assume that the 2DEG has vanishing thickness in the z direction when computing the scattering rate. With these approximations the imaginary part of the inverse dielectric function is calculated in the random-phase approximation from the configuration of the 2DEG electronic states (see the Appendix).

The scattering-probability distribution $\theta(p_\alpha,p_{\alpha'},\mathbf{P},\mathbf{P}')$ in Eqs. (1) and (2) is calculated by using Eqs. (3)–(5). Conservation of energy and momentum in the x,y direction assigns to every initial and final hot-electron state a specific excitation in the 2DEG. The energy of the excitation in terms of the initial and final momenta of the hot electron is

$$\hbar\omega=\frac{1}{2m^*}[p_\alpha^2-p_{\alpha'}^2+\mathbf{P}^2-\mathbf{P}'^2] = \frac{1}{2m^*}[p_\alpha^2-p_{\alpha'}^2+2P\hbar q\cos\gamma-\hbar^2q^2], \tag{6}$$

with $P\equiv|\mathbf{P}|$, $\hbar\mathbf{q}=\mathbf{P}-\mathbf{P}'$, $q\equiv|\mathbf{q}|$, where γ is the angle between the initial hot-electron momentum $\mathbf{P}$ and the momentum of the 2DEG excitation $\hbar\mathbf{q}$ (see Fig. 2). The angle γ can vary freely between 0 and 2π due to the rotational symmetry with respect to the z direction.

In evaluating the forward-scattering probability $P^>(E_c,E_i,\phi)$ in Eq. (1), we only consider positive energy change along the z direction, i.e., $\Delta E_z\equiv(p_\alpha^2-p_{\alpha'}^2)/2m^*>0$, as we are interested in the number of electrons scattering into the base, instead of the total number of scattered electrons. The particular $(\mathbf{q},\omega)$ state of the 2DEG that the hot electron excites by the scattering event can be indicated on the 2DEG excitation-spectrum diagram in Fig. 3. The area enclosed by the lines (i), (ii), and the q axis is the region of all the possible energy and lateral-momentum exchanges $\hbar\mathbf{q}$ of the hot electron for a particular initial state $|p_\alpha,\mathbf{P}\rangle$ to final state $|p_{\alpha'},\mathbf{P}-\hbar\mathbf{q}\rangle$. The two lines (i) and (ii) are given by Eq. (6) with the values for γ being 0 and π, respectively. These values for γ correspond to momentum exchange parallel or antiparallel to the lateral momentum $\mathbf{P}$ in the plane of the 2DEG. The intersection point of lines (i) and (ii) with the ω axis, point a, and the intersection points of lines (i) and (ii) with the q axis, points c and b, respectively, in Fig. 3 are given by

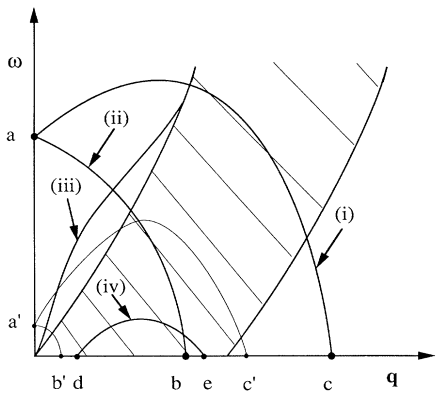

FIG. 3. The 2DEG excitation spectrum, with the hatched area indicating the Landau damping region, and curve (iii) the plasmon-dispersion curve [see Eq. (9)]. The region abc, circumscribed by curves (i) and (ii) and the q axis, includes excitations that the down-scattered hot electrons can bring about in the 2DEG by impinging on it; this leading to their down scattering. The area $a'b'c'$, enclosed by the faint lines, includes the excitations caused by a near 90° incident and down-scattered hot electrons. The excitations an upscattering electron can cause are encompassed by the line (iv) and the d-e part of the q axis. The equations for lines (i)–(iv) and points a–e are given in the text.

$$q_a=0,\quad \omega_a=\frac{p_\alpha^2-p_{\alpha'}^2}{2m^*\hbar}\quad\text{(point } a\text{)}, \tag{7a}$$

$$\hbar q_b=-P+[P^2+(p_\alpha^2-p_{\alpha'}^2)]^{1/2},\quad \omega_b=0\quad\text{(point } b\text{)}, \tag{7b}$$

$$\hbar q_c=P+[P^2+(p_\alpha^2-p_{\alpha'}^2)]^{1/2},\quad \omega_c=0\quad\text{(point } c\text{)}. \tag{7c}$$

As a function of the in-plane momentum $\mathbf{P}$, different $(\mathbf{q},\omega)$ 2DEG excitations can be brought about. To find the scattering probability $P^>(E_c,E_i,\phi)$, the scattering distribution $\theta(p_\alpha,p_{\alpha'},\mathbf{P},\mathbf{P}')$ has to be integrated over all the $\mathbf{P}'$ and $p_{\alpha'}>0$ states with $E_z(p'_\alpha)<E_c$. For a finite incidence angle, $\mathbf{P}\neq\mathbf{0}$, the integration over all $\mathbf{P}'$ extends over the area enclosed by the two lines (i) and (ii) (see Fig. 3). Note that as $|\mathbf{P}|$ increases (i.e., incident angles further from the normal), the intersection points b and c move further apart. For normal incidence, $\mathbf{P}=\mathbf{0}$, the points b

and c are the same and the integration is over a line extending from a to b. This case was treated by us previously.[5] The integration over the $p_{\alpha'}$ states is performed after the $\mathbf{P}'$ integration, as the $\mathbf{P}'$ integration area is dependent on the value of the outscattering momentum $p_{\alpha'}$. For diminishing change ΔE_z of the energy in the z direction, the integration area over the $\mathbf{P}'$ momenta of the outscattering states becomes smaller as the points a, b, and c recede towards the origin (indicated in Fig. 3 by points a', b', and c').

Using Eqs. (3)–(5), the energy loss in Eq. (2) is calculated as contributions of two parts. The first part involves integration over all the down-scattering states $|p_{\alpha'},\mathbf{P}'\rangle$, for which $\Delta E_z>0$. This proceeds analogously to the evaluation of the base scattering probability discussed above, except for the fact that the integrand is weighted with the energy loss associated with every down-scattering event. The second part accounts for the up-scattering contribution to the energy loss for which $\Delta E_z<0$. The integration over the hot-electron outscattering states is accordingly different from the down-scattering case: the integration over the z-direction outscattering momentum $p_{\alpha'}$ is from p_α to $(p_\alpha^2+\mathbf{P}^2)^{1/2}$, including all scattering possibilities from the case that all lateral momentum is given to the 2DEG (which determines the lower limit to the integration), to the case that all the lateral momentum is transferred to the z direction (which sets the upper limit). Given the initial and final momenta p_α and $p_{\alpha'}$, the integration over all the possible lateral outscattering momenta $\mathbf{P}'$ has to be performed. As with the calculation of the down-scattering contribution, this integration is performed by using excitation energy $\hbar\omega$ and the momentum exchange $\hbar\mathbf{q}$ variables defined by conservation of energy in Eq. (6) and momentum conservation in the x,y direction. With these variables the different scattering events can be depicted on a q,ω plane as in Fig. 3. The possible energy and momentum exchanges are restricted to the area within the arc joining the two points d and e [line (iv)], and the q axis in Fig. 3. This line is described by Eq. (6) with $\gamma=0$ and the appropriate values of p_α, $p_{\alpha'}$, and $\mathbf{P}$. Points d and e in Fig. 3 are given by

$$\hbar q_d=P-[P^2+(p_\alpha^2-p_{\alpha'}^2)]^{1/2},\quad \omega_d=0\quad(\text{point } d)\,,$$
$$\hbar q_e=P+[P^2+(p_\alpha^2-p_{\alpha'}^2)]^{1/2},\quad \omega_e=0\quad(\text{point } e)\,. \tag{8}$$

For decreasing values of ΔE_z, as happens when, e.g., $|\mathbf{P}|$ decreases, these two points move closer together.

The 2DEG excitation spectrum consists of a region in $(\mathbf{q},\omega)$ space of single-electron excitations and a collective plasmon-excitation curve (see the Appendix). The single-electron excitations are bounded by the energy and momentum conservation to the hatched area in Fig. 3.[6] The plasmon excitations along the curve (iii) are found as zeros of the dielectric function of the 2DEG. The plasmon dispersion curve is found analytically to be (see the Appendix)

$$\omega(q)^2=\frac{\hbar^2 q}{64m^{*2}a^*}\times\frac{[q^4a^{*2}+4q^3a^*+16k_F^2][q^2a^{*2}+4qa^*+4]}{[1+qa^*/4]}\,, \tag{9}$$

with $a^*\equiv 4\pi\epsilon_0\epsilon_r\hbar^2/m^*e^2$. The plasmon dispersion curve for small q varies as $\sqrt{q}$, and is nearly linear for larger q, before it enters the region of single-electron excitations, where the plasmons are Landau damped.

III. RESULTS

We proceed now to the calculation of the scattering probability and the energy loss for an electron traversing at oblique angle through a zero-temperature, one-subband 2DEG in GaAs with a sheet electron density of $n_s=10^{16}$ m^{-2} and effective mass m^* of 0.067 times the bare-electron mass, for varying injection and collection energies. This work goes beyond the earlier work by Gumbs and Horing[7] on electron scattering by a quantum electron slab in that we not only determine the energy loss, but also calculate the scattering probability. In fact we obtain both the total scattering probability and energy loss as functions of the injection energy and incidence angle (i), the base scattering probability as a function of the collection energy and incidence angle for a fixed injection energy (ii), and of the injection energy and collection energy for the perpendicular electron transport through a 2DEG (iii). From the latter case, (iii), it is possible to distinguish between those angular dependences in the scattering probability and energy loss which depend on the lowering of the energy in the z direction, and those which arise from genuinely directional dependences.

The total scattering probability for the forward- and backward-scattering cases as well as the energy loss for five different injection energies as a function of the incidence angle are shown in Figs. 4(a)–4(c). The presented total scattering probability is the fraction of injected electrons being scattered for a collection energy equal to the injection energy. The total scattering probability as well as the energy loss, for high energies of incidence (i.e., above approximately 100 meV) increases as the inverse cosine of the angle of incidence: the scattering probability is determined in part by the time the electrons take to cross the 2DEG. The larger the angle of incidence, the smaller the velocity in the z direction (by a factor $\cos\phi$), and the longer the electron takes to pass through the 2DEG. For lower energies of incidence this rule initially applies for low incidence angles, but because of drastic changes in the scattering phase space it fails for larger incidence angles. The larger incidence angle makes it energetically impossible to excite plasmons. The plasmon contribution to the scattering probability is plotted in the inset of Fig. 4(a). After the disappearance of the plasmon-scattering channel only the single-electron excitations contribute to the hot-electron scattering process, whose rate increases with higher incidence angles due to the longer dwell time. To put it otherwise, at increasing angles of incidence, the area of integration in the $(\mathbf{q},\omega)$

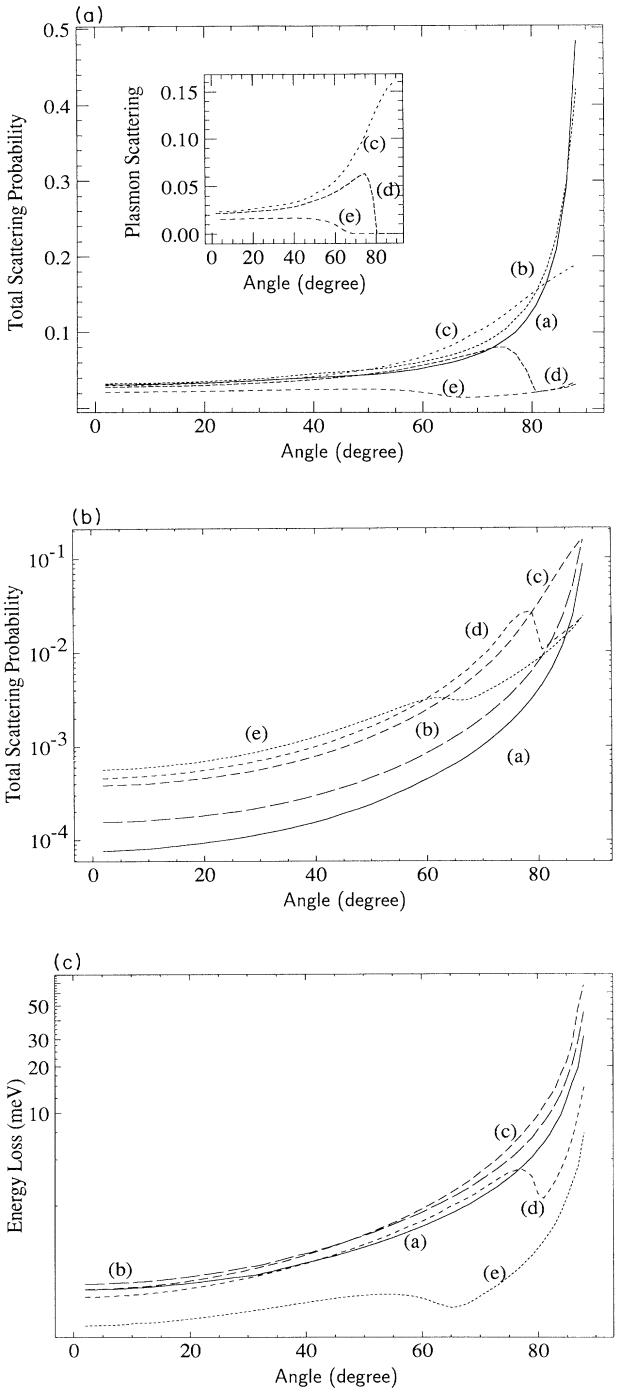

FIG. 4. (a) The total forward-scattering probability of an electron of a given incidence energy passing through a 2DEG (electron density $n_s = 10^{16}$ m^{-2}) as a function of incidence angle. The injection energies are (*a*) 300, (*b*) 200, (*c*) 100, (*d*) 80, and (*e*) 50 meV. The corresponding total backward-scattering probability and energy loss are shown in (b) and (c), respectively. The inset in (a) shows the plasmon contribution to the scattering probability for curves (*c*)–(*e*). For large incidence angles the plasmon-scattering channel disappears at incidence energies below approximately 100 meV. Note that the plasmon-scattering contribution to the scattering probability decreases sharply for 80 meV injection energy [see the inset in (a)].

excitation space of the 2DEG eventually grazes the plasmon-dispersion curve and subsequently no longer encompasses it, at which point the scattering probability decreases sharply. The same qualitative effects can also be observed in the backward-scattering probability and the energy loss.

In Fig. 5 we show the scattering probability, for an incidence energy of 300 meV as a function of incidence angle for collection energies 50, 100, and 200 meV. The energy in the z direction decreases monotonously for increasing angle of incidence. Eventually this energy is less than the collection energy at which instant the electrons trap in the base. For a given collection energy smaller than the injection energy, the scattering probability remains small. It is only when the energy in the z direction, E_z, is about the collection energy that the scattering probability increases dramatically. This feature is due to the dominance of small-energy-loss scattering events for the hot-electron–2DEG interaction, as can be understood from Fig. 3. Large-energy-loss scattering events correspond to high-energy single-electron and plasmon excitations that have small scattering amplitudes. By contrast, when the energy loss of the hot electron is small, both plasmons with larger scattering amplitudes and low-energy single-electron excitations are involved.

In Fig. 6(a) we show the base scattering probability for transport through a 2DEG for four different collection energies. The plain curve is the total scattering probability as a function of incident energy. The lower curves are the fraction of electrons being scattered below a certain collection energy. Once the collection energy is sufficiently below the injection energy, the scattering probability falls dramatically, indicating again that the largest part of the scattering occurs by small-energy-loss processes and small-angle scattering as discussed above. In Fig. 6(b) the difference between the sum of the total

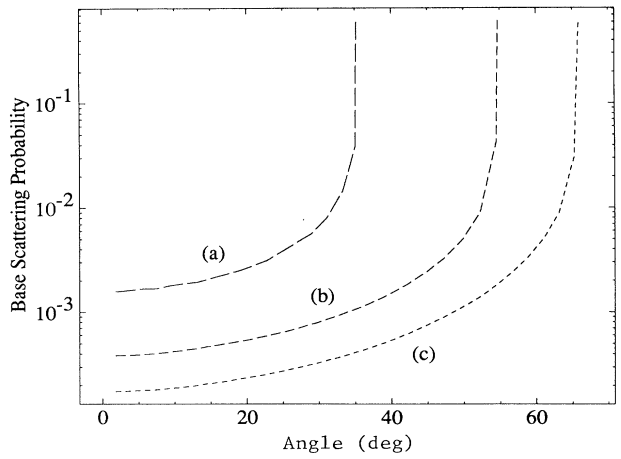

FIG. 5. The base scattering probability for a 300-meV hot electron impinging on a 2DEG ($n_s = 10^{16}$ m^{-2}) as a function of incidence angle and for collection energies of (*a*) 200, (*b*) 100, and (*c*) 50 meV. The right-most part of the curves corresponds to the angles at which the energies in the z direction are equal to the collection energies.

forward- and backward-scattering probabilities and the semiclassical scattering probability is shown. The latter is calculated by multiplying the total scattering probability calculated for perpendicular incidence as a function of incidence energy, as shown in Fig. 6(a) curve (*a*), with the inverse-cosine of the incident angle. Deviations of the scattering probability as a function of incidence angle become prominent for injection angles above approximately 40°. This discrepancy is due to the change in the scattering geometry, which changes from mainly perpendicular to mainly parallel electron injection. These are classically the same but quantum mechanically different. Below 100 meV injection energy, large deviations from the semiclassical inverse-cosine behavior occur due to the loss of the plasmon-scattering channel as discussed in connection with Fig. 4.

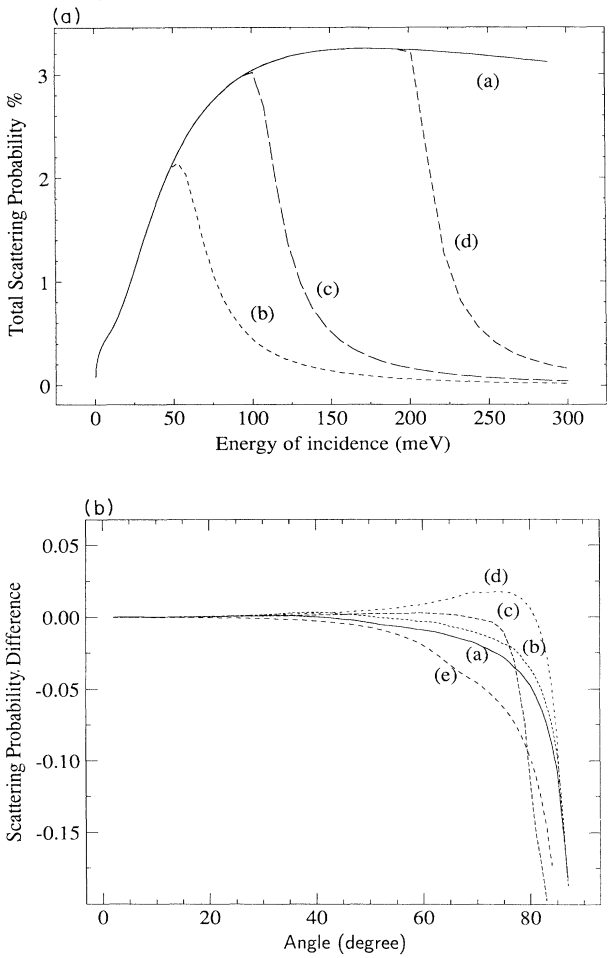

FIG. 6. (a) The total base scattering probability (*a*), and the base scattering probability of hot electrons passing perpendicularly through a 2DEG (electron density $n_s = 10^{16}$ m^{-2}) as a function of injection energy for collection energies of (*b*) 50, (*c*) 100, and (*d*) 200 meV. (b) shows the difference between the sum of the quantum-mechanical total forward- and backward-scattering probabilities from the semiclassical result (quantum-mechanical minus semiclassical). The latter is obtained by multiplying the total scattering probability, shown as curve (*a*) in (a), by the inverse cosine of the incidence angle. The differences between the quantum-mechanical and the semiclassical scattering probabilities are shown for (*a*) 300, (*b*) 200, (*c*) 100, (*d*) 80, and (*e*) 50 meV injection energies.

Finally we discuss the implications of the above results for the operation of the 2DEGBHET. Figure 6(a) shows that the scattering present in this device is due largely to the small-energy-loss processes for the hot-electron–2DEG interaction. By applying a magnetic field parallel to the 2DEG, the injected electrons in this device are bent round so that they impinge with a finite angle on the 2DEG. In the absence of electron–LO-phonon scattering processes, the base scattering probability for a 300-meV injection-energy electron will take a form similar to those shown in Fig. 5, corresponding to three different collector barrier heights. For a base of thickness l, an injection energy E_i (equal to $\frac{1}{2}m^* v_i^2$ with v_i the speed of incoming electrons), and a magnetic field B weak enough that the electrons still impinge on the 2DEG, the angle of incidence is given by $\phi = \sin^{-1}(leB/m^* v_i)$. The presence of the electron–LO-phonon scattering processes will change the fraction of electrons scattering into the base from those shown in Figs. 4–6. If the base-collector barrier is at least one LO-phonon energy below the injection energy, we expect that our calculated hot-electron–2DEG scattering processes will be observed. The LO-phonon scattering probability decreases very sharply for two or more scattering processes in the base.[8] The scattering probabilities in Figs. 5 and 6 should be experimentally measurable. The dip in the scattering probability in Fig. 4(a) [branch (*e*)] will be difficult to observe experimentally for several reasons. First, the angle at which the dip occurs is large, requiring a low base-collector barrier, thus a large base-collector voltage, leading to leaking currents which make it difficult to detect the contribution of injected electrons to the collector current. Second, those injected electrons scattered by LO phonons into the base will make it hard to distinguish between energy loss from phonon or electron interactions. Detailed and quantitative comparison of the results of the present theory with the experimental measurements on a 2DEGBHET will be published elsewhere;[9] preliminary indications are that we underestimate the scattering rate for oblique incidence with our present theory, although it agrees well for near-normal incidence of the hot-electron injection.

IV. SUMMARY

We have calculated the scattering rate and energy loss as functions of emitter and collector biases and angle of incidence for electrons impinging on a 2DEG with an electron-sheet density $n_s = 10^{16}$ m^{-2} in GaAs. By varying these we have shown how different areas of the 2DEG excitation spectrum contribute to the scattering rate. The scattering probability and energy loss as functions of incidence angle increase, for high energies of incidence, semiclassically for angles below 40°. For larger incidence angles deviations from the semiclassical result are observable. At low injection energies E_i smaller than 100 meV, which is incidentally the collection energy in our calcula-

tions, the scattering probability can decrease due to the disappearance of the plasmon-scattering channel. The base scattering probability as a function of energy of incidence has been calculated and it has been shown that a high injection energy is required to obtain high amplification factor for the 2DEGBHET, i.e., little loss. Future work includes the investigation of the role of plasmon-phonon coupling in the hot-electron–2DEG interaction.

ACKNOWLEDGMENTS

R.-J.E.J. would like to thank Paul Matthews for helpful discussions and acknowledges financial support of Trinity College, Cambridge. B.F. thanks Girton College, Cambridge, for support. This work was supported in part by the Science and Engineering Research Council and the Department of Trade and Industry, U.K.

APPENDIX

The imaginary part of the inverse of the dielectric function, also known as the loss function, can be found from the dielectric function by making use of the relation between the dielectric function and its inverse,

$$\int_{-L_z/2}^{L_z/2}\epsilon(z,z',\mathbf{q};\hbar\omega)\epsilon^{-1}(z',z'',\mathbf{q};\hbar\omega)dz'=\frac{\delta(z-z'')}{(L_xL_y)^2}\ . \tag{A1}$$

The dielectric function $\epsilon(z,z',\mathbf{q};\hbar\omega)$ of the 2DEG can be found from the corresponding polarization function $P(\mathbf{q};\hbar\omega)$ as follows:

$$\epsilon(z,z',\mathbf{q};\hbar\omega)=\frac{\delta(z-z')}{L_xL_y}\int_{-L_z/2}^{L_z/2}\frac{V(z-z'',\mathbf{q})|\phi(z'')|^2|\phi(z')|^2P(\mathbf{q};\hbar\omega)dz''}{L_xL_y}\ , \tag{A2}$$

where $V(z-z'',\mathbf{q})\equiv e^2\exp[-q|z-z''|]/(2\epsilon_0\epsilon_r q)$ is the Fourier transformed Coulomb potential; $q\equiv|\mathbf{q}|$, ϵ_0 is the permittivity of vacuum and ϵ_r the relative dielectric constant of the semiconductor. For the GaAs (base region) we take $\epsilon_r=13.1$. The polarization function of the 2DEG in the random-phase approximation has the following form:[10]

$$P(\mathbf{q};\hbar\omega)=\frac{m^*k_F}{2\pi^2\hbar^2q}\left[B\left[\frac{\omega}{qv_F}+\frac{q}{2k_F}\right]-B\left[\frac{\omega}{qv_F}-\frac{q}{2k_F}\right]\right]\ , \tag{A3}$$

with $B(b)\equiv-2\pi[b-\mathrm{sgn}(b)(b^2-1)^{1/2}]$, for $|b|>1$ and $-2\pi[b-i(1-b^2)^{1/2}]$, for $|b|\le1$. Here $v_F\equiv\hbar k_F/m^*$ is the Fermi velocity with k_F the Fermi wave number corresponding to the density of the 2DEG. Using the method employed in Ref. 11, the inverse dielectric function can be found to be

$$\epsilon^{-1}(z',z'',\mathbf{q};\hbar\omega)=\frac{\delta(z-z'')}{L_xL_y}+\frac{V(z',\mathbf{q})P(\mathbf{q};\hbar\omega)|\phi(z'')|^2}{[1-V(0,\mathbf{q})P(\mathbf{q};\hbar\omega)]L_xL_y}\ . \tag{A4}$$

For evaluating the imaginary part of the inverse of the dielectric function we distinguish between two cases, which are $P''(\mathbf{q};\hbar\omega)\not\to0$ and $P''(\mathbf{q};\hbar\omega)\to0$. Whereas the result of the former case is directly obtained, for the latter case we make use of the standard relation $1/(x+i\eta)=\mathrm{P}(1/x)-i\pi\,\mathrm{sgn}(\eta)\delta(x)$, in which $\eta\to0$ and P stands for the principal value. Noting that for $\omega>0$, $\mathrm{Im}[\epsilon^{-1}]\le0$, which implies $P''\uparrow0$, we obtain the result as given below. We have (note that both $q>0$ and $\omega>0$)

$$\mathrm{Im}[\epsilon^{-1}(z',z'',\mathbf{q};\hbar\omega)]=\begin{cases}\dfrac{V(z',\mathbf{q})P''(\mathbf{q};\hbar\omega)|\phi(z'')|^2}{[\{1-V(0,\mathbf{q})P'(\mathbf{q};\hbar\omega)\}^2+\{V(0,\mathbf{q})P''(\mathbf{q};\hbar\omega)\}^2]L_xL_y} & \text{when } -qv_F+\dfrac{\hbar q^2}{2m^*}<\omega<qv_F+\dfrac{\hbar q^2}{2m^*}\\ \dfrac{-\pi V(z',\mathbf{q})P'(\mathbf{q};\hbar\omega)|\phi(z'')|^2\delta(1-V(0,\mathbf{q})P'(\mathbf{q};\hbar\omega))}{L_xL_y} & \text{when } \omega>qv_F+\dfrac{\hbar q^2}{2m^*}\ ,\end{cases} \tag{A5}$$

and zero otherwise.

The first part of Eq. (A5), corresponding to $P''(\mathbf{q};\hbar\omega)\not\to0$, represents the loss function for the single-electron excitations. The hatched area in Fig. 3 denotes the region where single-electron excitations can take place. The second part of Eq. (A5), corresponding to $P''(\mathbf{q};\hbar\omega)\to0$, specifies the plasmon contribution to the loss function. The solution to the equation $1-V(0,\mathbf{q})P'(\mathbf{q};\hbar\omega)=0$, $1-V(0,\mathbf{q})P'(\mathbf{q};\hbar\omega)$ being the argument of the δ function in Eq. (A5), yields, when solved analytically, the plasmon-dispersion relation. This relation can be trivially obtained by substituting the real part of the polarization function in the region $q>0$ and $\omega>qv_F+\hbar q^2/2m^*$ from Eq. (A3) into the equation $1-V(0,\mathbf{q})P'(\mathbf{q};\hbar\omega)=0$. Squaring this equation twice to eliminate the square roots, the dispersion relation for the plasmons, as given in Eq. (9), is found.

[1]P. Matthews, M. J. Kelly, V. J. Law, D. G. Hasko, M. Pepper, H. Ahmed, D. C. Peacock, J. E. F. Frost, D. A. Ritchie, and G. A. C. Jones, Electron. Lett. **26**, 862 (1990).

[2]P. Matthews, M. J. Kelly, V. J. Law, D. G. Hasko, M. Pepper, H. Ahmed, D. C. Peacock, J. E. F. Frost, D. A. Ritchie, and G. A. C. Jones, Phys. Rev. B **42**, 11 415 (1990).

[3]P. Matthews, M. J. Kelly, D. G. Hasko, J. E. F. Frost, D. A. Ritchie, G. A. C. Jones, M. Pepper, and H. Ahmed, Semicond. Sci. Technol. **7**, B536 (1992).

[4]P. Matthews, M. J. Kelly, D. G. Hasko, H. Ahmed, J. E. F. Frost, D. A. Ritchie, and G. A. C. Jones, Surf. Sci. **263**, 141 (1992).

[5]R.-J. E. Jansen, B. Farid, and M. J. Kelly, Appl. Phys. Lett. **60**, 1881 (1992).

[6]D. Pines, *Elementary Excitations in Solids* (Benjamin, New York, 1963). The figure on p. 149 is equivalent to our Fig. 3 but corresponds to an isotropic electron-gas system. Note that in contrast to the two-dimensional case, the 3D plasmon curve does not pass through the origin.

[7]G. Gumbs and N. J. M. Horning, Phys. Rev. B **43**, 2119 (1991).

[8]S. A. Lyon and C. L. Peterson, Semicond. Sci. Technol. **7**, B21 (1992).

[9]P. Matthews, R.-J. E. Jansen, M. J. Kelly, B. Farid, D. G. Hasko, J. E. F. Frost, D. A. Ritchie, G. A. C. Jones, M. Pepper, and H. Ahmed (unpublished).

[10]T. Ando, A. B. Fowler, and F. Stern, Rev. Mod. Phys. **54**, 437 (1982).

[11]M. Ortuno and J. C. Inkson, J. Phys. C **12**, 1065 (1979).